AGU PUBLICATIONS

Geophysical Research Letters

RESEARCH LETTER
10.1002/2015GL066054

Key Points:
- Stratospheric zonally uniform tides are clearly observed during the Northern Hemisphere summer
- The characteristics can be mostly explained by the second, antisymmetric, propagating Hough mode
- Diurnal variations must be considered when calculating the climatological zonal mean field

Supporting Information:
- Text S1

Correspondence to:
T. Sakazaki,
takatoshi_sakazaki@rish.kyoto-u.ac.jp

Citation:
Sakazaki, T., T. Sasaki, M. Shiotani, Y. Tomikawa, and D. Kinnison (2015), Zonally uniform tidal oscillations in the tropical stratosphere, *Geophys. Res. Lett.*, *42*, 9553–9560, doi:10.1002/2015GL066054.

Received 3 SEP 2015
Accepted 14 OCT 2015
Accepted article online 21 OCT 2015
Published online 14 NOV 2015

©2015. American Geophysical Union. All Rights Reserved.

Zonally uniform tidal oscillations in the tropical stratosphere

Takatoshi Sakazaki[1], Takuya Sasaki[1], Masato Shiotani[1], Yoshihiro Tomikawa[2,3], and Douglas Kinnison[4]

[1]Research Institute for Sustainable Humanosphere, Kyoto University, Uji, Japan, [2]National Institute of Polar Research, Tachikawa, Japan, [3]SOKENDAI, Tachikawa, Japan, [4]National Center for Atmospheric Research, Boulder, Colorado, USA

Abstract By analyzing data from satellite measurements, a reanalysis, and a chemistry-climate model, we found clear zonally uniform tidal signals in the tropical stratosphere, particularly during the Northern Hemisphere summer. Antisymmetric components with respect to the equator are dominant and are characterized by a vertical wavelength of ~15 km and a diurnal frequency. The temperature and vertical wind diurnal amplitudes in the stratosphere are 0.2–1 K and 1–7 mm s^{-1}, respectively. The latter is generally larger than the climatological ascent motion in the stratosphere. The observed latitudinal and vertical structures can be explained by the second, propagating, antisymmetric Hough mode. These tidal oscillations should be carefully considered in analyses of zonal mean fields at a particular universal time.

1. Introduction

Atmospheric tides are global-scale waves that are driven by the diurnally varying diabatic heating rate in the troposphere and the stratosphere [*Chapman and Lindzen*, 1970]. Although tidal variations are dominant in the mesosphere and lower thermosphere (MLT) regions, they also have a significant amplitude in the stratosphere [e.g., *Sakazaki et al.,* 2012]. Stratospheric tides change the distribution of atmospheric minor constituents [*Sakazaki et al.,* 2013a], while the accurate estimate of tides is important for the correction of "diurnal drift effects" in satellite measurement data [*Zou et al.,* 2014].

The present study focuses on one of the nonmigrating (non-Sun-synchronous) tidal components, the zonally uniform tides (i.e., tides with zonal wave number 0), since they are crucial for meteorological analyses from a practical perspective. That is, stratospheric general circulation, such as Brewer-Dobson circulation (BDC), is often assessed by means of the climatological (e.g., monthly) zonal mean field. Diurnal variations in the zonal mean field, if any, should be carefully removed to obtain accurate estimates. *Seviour et al.* [2012] noted that the zonal mean vertical velocity, and consequently the residual circulation, is strongly correlated with the universal time (UT). Although they did not examine the responsible phenomena in detail, it is expected that zonally uniform tides have a significant amplitude in the stratosphere. Note that all other components, including migrating (Sun-synchronous) tides, are identically zero when the zonal mean is taken at a particular UT.

Previous studies of zonally uniform tides mostly considered the MLT [e.g., *Hagan and Roble*, 2001; *Oberheide et al.,* 2002; *Forbes and Wu*, 2006]. In the stratosphere, *Lieberman* [1991] first detected diurnal, zonally uniform tides using data from the Nimbus 7 Limb Infrared Monitor of the Stratosphere. Note that the original analysis of *Lieberman* [1991] was restricted to the period from October to April and seasonality was not examined. *Lieberman and Leovy* [1995] showed that the observed features could be reasonably reproduced by classical tidal modeling. Zonally uniform tides appearing in a general circulation model (GCM) were examined by *Chiba and Shibata* [1992] and *Kuroda and Chiba* [1995]. Recently, *Sakazaki et al.* [2015] (hereafter S15) demonstrated the full picture of nonmigrating tides in the tropical stratosphere. They found clear gravity wave patterns emanating from the two major continents, Africa and South America. In addition, the potential energy (PE) associated with the zonally uniform diurnal tides is strong, particularly during the Northern Hemisphere (NH) summer; however, the corresponding signals were not clear in the nonmigrating tides extracted and averaged between 10°S and 10°N (i.e., the symmetric components with respect to the equator; see their Figure 6). These apparently contradictory results may indicate that the antisymmetric components attain a significant amplitude in the context of zonally uniform tides.

The purpose of this study is to investigate the zonally uniform tides in the tropical stratosphere, including their latitudinal-vertical structures and their seasonality, using satellite measurements, reanalyses, and a chemistry-climate model (CCM). We demonstrate that zonally uniform tides are clearly observed, particularly during the NH summer season, with characteristic latitudinal and vertical structures. The remainder of this

paper is organized as follows. Section 2 describes the data sets used and analysis methods employed. Section 3 presents the results and discusses their relationship to tropospheric diabatic heating. Finally, the main findings are summarized in section 4.

2. Data and Analysis Methods

2.1. Data Sets

Data from two independent satellite measurements, a reanalysis (JRA-55) and a CCM (WACCM), were analyzed for the period 2008–2010.

As for the satellite measurements, we analyzed temperature data from the Sounding of the Atmosphere using Broadband Emission Radiometry (SABER) instrument on board the Thermosphere-Ionosphere-Mesosphere Energetics and Dynamics satellite [*Russell et al.,* 1999] and from Global Positioning System radio occultation measurements of the Constellation Observing System for Meteorology, Ionosphere, and Climate (COSMIC)/FORMOSAT-III mission [*Anthes et al.,* 2008]. As regards SABER, version 2.0 temperature data on pressure levels were analyzed for the latitude region between 50°S and 50°N; as for COSMIC, dry-temperature data on geometric altitude levels, compiled by the COSMIC Data Analysis and Archival Center (CDAAC), were analyzed.

JRA-55 is the second Japanese global atmospheric reanalysis conducted by the Japan Meteorological Agency (JMA) [*Kobayashi et al.,* 2015]. Data are provided 6-hourly for 37 pressure levels between 1 hPa and 1000 hPa, with a horizontal spacing of $1.25° \times 1.25°$. JRA-55 products are considerably better than the JRA-25 product, which was the first version of the JMA reanalysis [*Onogi et al.,* 2007]. Note that COSMIC data are assimilated into the JRA-55 system, whereas SABER data are not.

For JRA-55, diabatic heating rates for 2008 were also analyzed. The heating rates include heating by convection, large-scale condensation, solar and long-wave radiation, and vertical diffusion processes. Data are provided 4 times daily, as averages for 0000–0600 UTC, 0600–1200 UTC, 1200–1800 UTC, and 1800–2400 UTC. For the classical tidal modeling approach (section 3.2), the data below 500 hPa level were assumed to decrease linearly to zero at 1000 hPa level.

The National Center for Atmospheric Research (NCAR) Whole Atmosphere Community Climate Model, version 4 (WACCM4), is a comprehensive numerical model spanning the range of altitude from the Earth's surface to the thermosphere [*Marsh et al.,* 2013]. WACCM4 is based on the framework of the NCAR Community Atmosphere Model, version 4 (CAM4), and includes all of the physical parameterizations of CAM4 [*Neale et al.,* 2013]. In this study, model results are used for the 2008–2010 period based on the Chemistry Climate Model Initiative REFC1 scenario [*Eyring et al.,* 2013]. Model results are provided at 3 h intervals on 66 sigma-pressure (σ-p) levels between the surface and 5.96×10^{-6} hPa. The horizontal resolution used for this work is $1.9° \times 2.5°$.

2.2. Analysis Methods

We extracted zonally uniform tides averaged for each month or for each season (i.e., December-January-February (DJF), March-April-May (MAM), June-July-August (JJA), or September-October-November (SON)) using the 3 year data set.

The analysis procedure adopted for JRA-55 and WACCM is as follows. Six-hourly (for JRA55) or 3-hourly (for WACCM) daily anomaly components were extracted by taking averages at each UT, followed by subtraction of their daily mean values. The zonally uniform tides were then extracted by taking the zonal mean of the daily anomaly for each latitude band at each UT. The uncertainty is also estimated (see Text S1 in the supporting information for details).

Our analysis of the SABER data basically followed the method adopted by S15. We derived hourly daily-anomaly components in bins of 24° in longitude, 5° in latitude, and 2 km between 20 km and 120 km in vertical log-pressure coordinate. Note that background-temperature changes were removed before analysis (see S15 for details). Then, zonally uniform tides were extracted by taking the zonal mean of the daily anomalies.

Finally, because the measurement locations and times are random, COSMIC data were averaged in bins of 5° in latitude, 2 km in geometric altitude below 35 km, and 3 h in time (UT). The daily mean was calculated at each grid point by averaging the data over 24 h. Then, the daily mean was subtracted from the original 3-hourly data, so that 3-hourly zonally uniform tides were obtained.

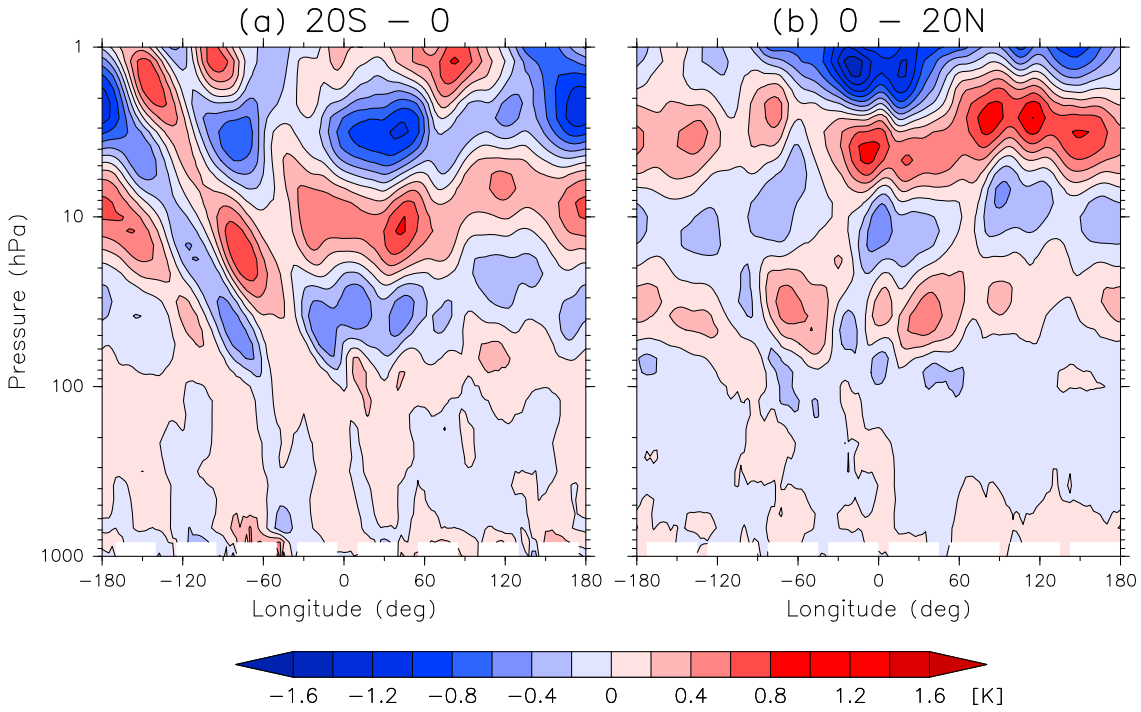

Figure 1. Longitude-altitude distribution of all nonmigrating temperature tides at 0000 UTC in July, averaged between (a) 20°S and 0°N/S and (b) 0°N/S and 20°N, as derived from WACCM data for 2008–2010.

For the 3-hourly WACCM data, all nonmigrating tides, including the zonally uniform tides, were also extracted using the method proposed by S15. In the application of this method, nonmigrating tides are obtained in physical space by taking the difference between all tidal components and the migrating tidal components (see S15 for details).

3. Results and Discussion

3.1. General Characteristics

Figure 1 shows the longitude-altitude distribution of all nonmigrating tides in temperature in July, averaged between 20°S and 0°N (Figure 1a) and 0°N and 20°N (Figure 1b), derived from WACCM data. Zonally uniform patterns are clear, in addition to the gravity wave-like pattern emanating from the two major continents (Africa and South America) that was discovered by S15. For the zonally uniform pattern, the phase is almost opposite between the NH and the Southern Hemisphere (SH); e.g., positive (negative) values prevail at 10 hPa in the NH (SH), indicating a strong antisymmetric structure with respect to the equator (hereafter, these are simply called antisymmetric components). Note that S15 revealed a picture of nonmigrating tides averaged over the latitudinal band between 10°S and 10°N (Figure 6 of S15), so that any "antisymmetric" components were not clear, while the PE averaged over the same region attains large values.

In the following, the zonally uniform tides are extracted and discussed. Figure 2 shows the latitude-altitude distribution of zonally uniform tides in temperature and vertical wind in log-pressure coordinate, from several data sets obtained during JJA. All data sets are in good agreement in the sense that the antisymmetric components are dominant, thus creating a patchy pattern. Note that meridional wind shows a symmetric structure (not shown), being consistent with the finding in a GCM study by *Kuroda and Chiba* [1995]. The diurnal amplitudes for temperature and vertical wind are found to be 0.2–1 K and 1–7 mm s^{-1}, respectively, although there is a difference in vertical wind amplitude (1–2 mm s^{-1}) in the upper stratosphere between WACCM and JRA-55. The 95% significance level for the deduced amplitude in temperature (vertical wind) is ±0.05 K (±0.7 mm s^{-1}) at 100 hPa, ±0.06 K (±0.5 mm s^{-1}) at 10 hPa, and ±0.13 K (±1.7 mm s^{-1}) at 1 hPa, at 10°N for JRA55. The phase pattern shows a clear downward progression with time (not shown), indicating upward energy propagation. The variations in temperature precede those in vertical wind by a quarter cycle, satisfying the thermodynamic equation for the adiabatic case. The vertical wavelength (λ_z) is estimated at ~15 km in the stratosphere.

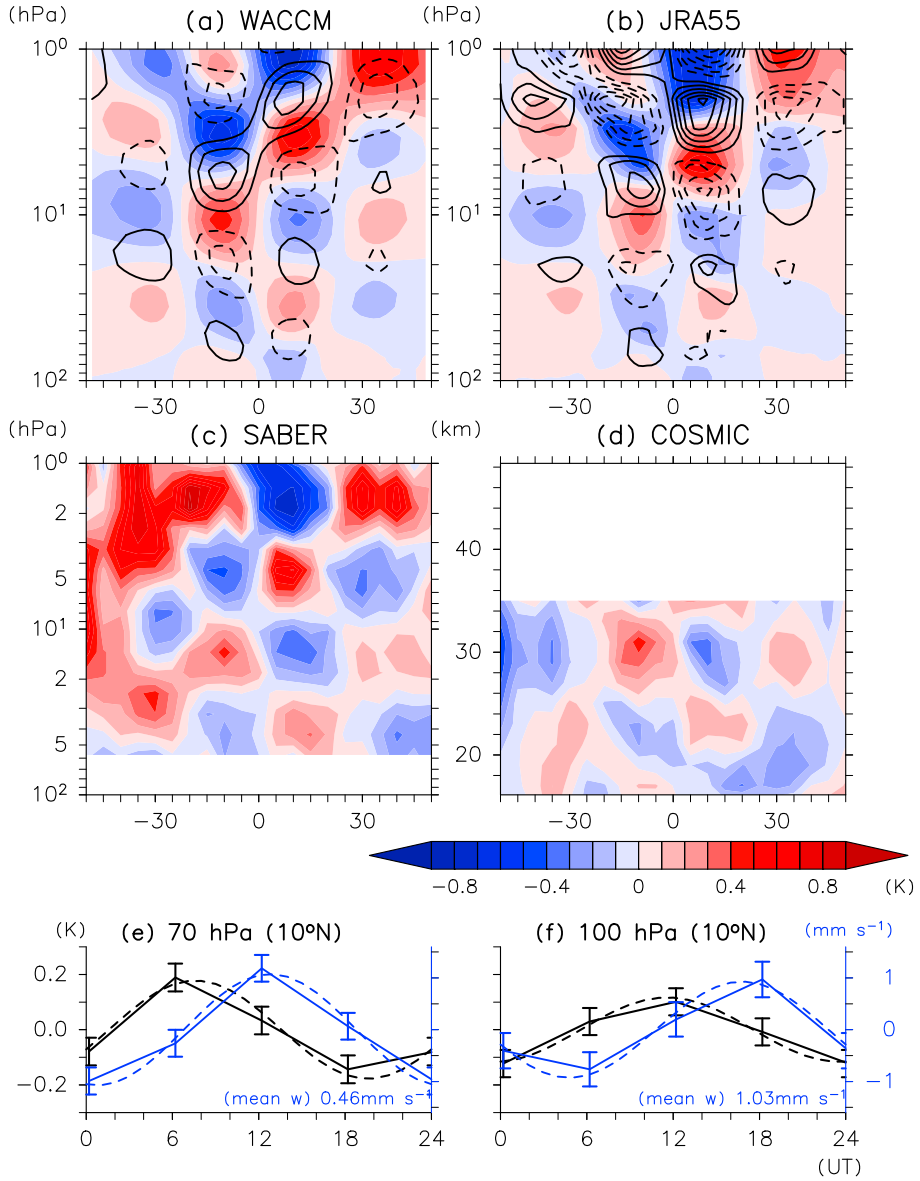

Figure 2. Latitude-altitude distribution of the zonally uniform tidal temperature (color shading) and the vertical wind in log-pressure coordinate (contours) at 0000 UTC during JJA, as derived from (a) WACCM, (b) JRA-55, (c) SABER, and (d) COSMIC data. For Figures 2a and 2b, the contour interval for the vertical wind is 1 mm s^{-1}. Zonally uniform tides at (e) 70 hPa and (f) 100 hPa at 10°N during JJA, as derived from JRA55 data. Black and blue solid curves are for temperature and vertical velocity in log-pressure coordinate, respectively. Dashed curves denote best fits to the diurnal harmonic component. The horizontal bars denote 95% confidence levels with *t* test (see text for details).The zonal mean and climatological mean vertical velocities are also shown in each panel.

Figures 2e and 2f show the time series of zonally uniform tides at 100 hPa and 70 hPa, respectively, for the temperature and vertical wind at 10°N during JJA. These pressure levels are important for BDC as the "gate" to the stratosphere [*Fueglistaler et al.,* 2009]. The peak-to-peak difference for the temperature is ~0.2 K (0.4 K) at 100 hPa (70 hPa) and that of the vertical velocity is 2 mm s^{-1} (2.5 mm s^{-1}) at 100 hPa (70 hPa). As regards the vertical velocity, the diurnal variations are larger than the climatological mean values (1.03 and 0.46 mm s^{-1} at 100 and 70 hPa, respectively), which means that even its sign (i.e., ascending or descending) changes within a day. Note that *Seviour et al.* [2012] speculated that the semidiurnal component is dominant, based on their finding that the sign of the vertical wind is opposite between 0600 and 1200 UTC at 70 hPa (cf., Figure 2e). The present results, however, reveal that the diurnal component is dominant, as shown by

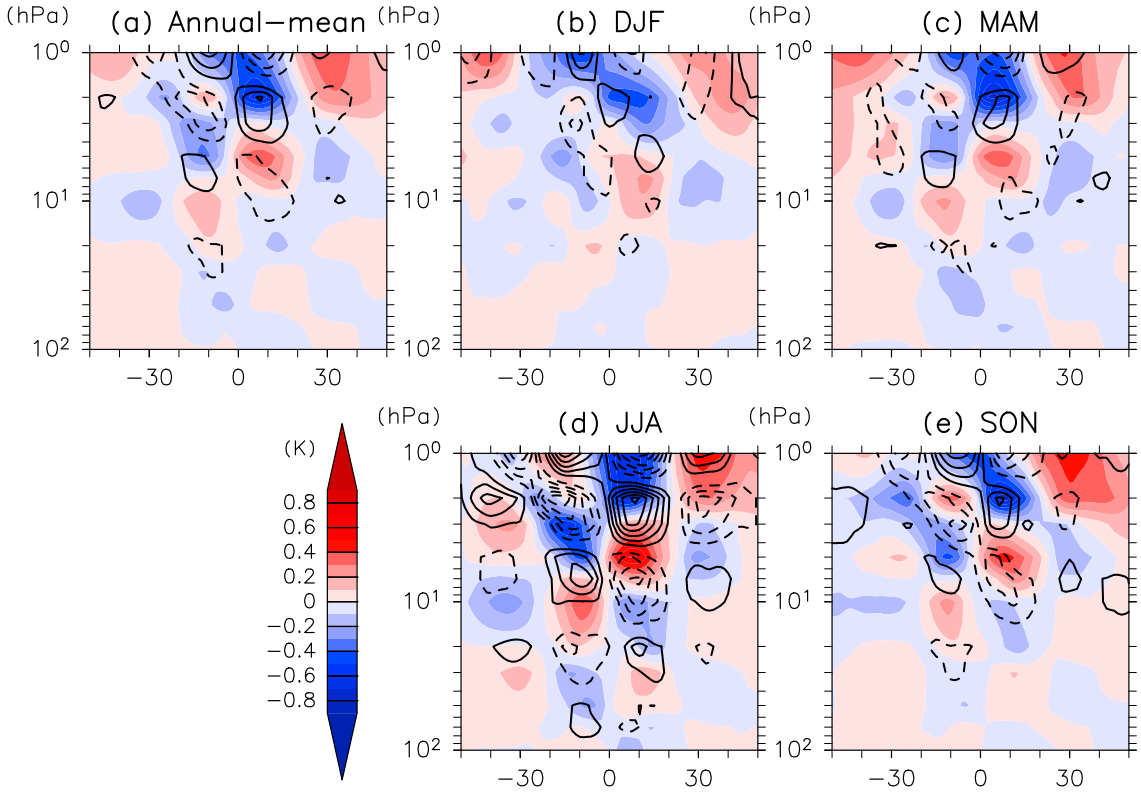

Figure 3. As for Figure 2b, but for (a) the annual mean, (b) DJF, (c) MAM, (d) JJA, and SON during 2008–2010, as derived from JRA-55 data.

the curve fitted to the diurnal harmonic (dashed curve); the opposite sign occurs owing to the diurnal component. Consequently, the diurnal component is considered later, in section 3.2.

Results for other seasons are shown in Figure 3, based on JRA55 data. The other data sets yield similar results (not shown). The zonally uniform tides are strongest during JJA and weakest during DJF. During MAM and SON, the amplitude is weaker than that during JJA, but the antisymmetric components are still dominant. Note that annual mean zonally uniform tides (Figure 3a) are also characterized by antisymmetric components, reflecting strong signals during JJA.

3.2. Hough Mode Decomposition

Hough mode decomposition is a useful tool for understanding the latitude-altitude structure of the tides. The zonally uniform tides characterized by the diurnal frequency (D0) are expressed through a superposition of Hough modes,

$$T = \sum_n C_n(z)\Theta_n(\theta)\exp(i\omega t), \tag{1}$$

where C_n is the complex coefficient, Θ_n is the nth Hough function (which is a function of latitude, θ), ω is the diurnal frequency, and t is UT.

Figure 4a shows the shapes of the propagating Hough modes for the D0 tide. Here we consider propagating modes, because we focus on clear signals in the tropics. The first and second modes for each of the symmetric and antisymmetric modes are shown. In the following, we express the ith propagating (trapped), symmetric (antisymmetric) mode as "P(T)-S(A)-i mode." Figure 4b shows the zonally uniform tidal temperature at 0000 UTC, 5 hPa in July, derived from JRA-55 data. The observed latitudinal structure can be approximately explained by the P-A-2 mode, as shown by the best fitting curve for this single mode. This is consistent with the finding by *Kuroda and Chiba* [1995]. The observed vertical wavelength (~15 km) is also consistent with the theoretically predicted wavelength for the P-A-2 mode of ~15 km (equivalent depth, $h_n \sim 0.23$ km) in the case of $N^2 = 4.0 \times 10^{-4}$ and $H = 7$ km, where N and H are the Brunt-Väisälä frequency and the scale height, respectively.

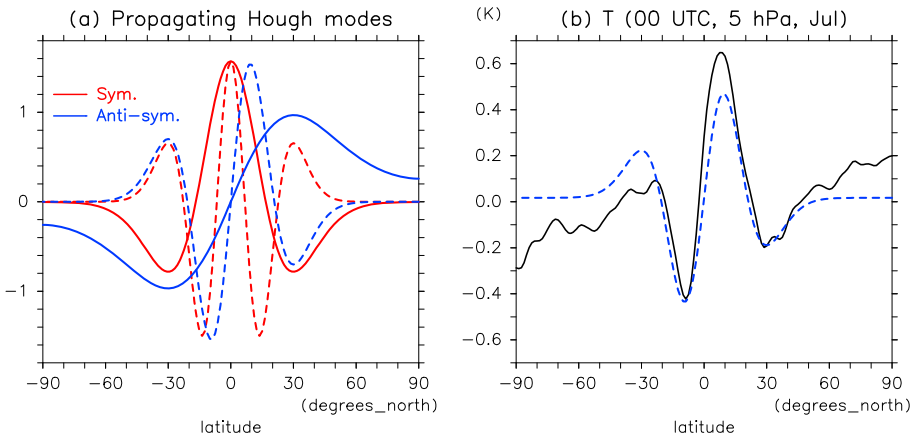

Figure 4. (a) Propagating Hough modes for the diurnal, zonally uniform (wave number 0) tide. Red and blue curves denote symmetric and antisymmetric components, respectively. Solid and dashed curves denote the first and second modes, respectively. (b) Temperature of zonally uniform tides at 0000 UTC at 5 hPa in July (black curve), derived from JRA-55 data obtained during 2008–2010, and best fitting curve to the second, antisymmetric Hough mode (blue dashed curve).

Figure 5a shows the seasonal variation of the amplitude of the Hough mode coefficient (i.e., $|C_n|$ in equation (1)) at 5 hPa during 2008, as derived from the JRA55 data. As expected from Figures 3 and 4, the P-A-2 mode attains a maximum during the NH summer. The amplitude is 2–3 times larger than that of the other modes. During the NH winter, in contrast, all modes have comparable amplitudes. This finding is consistent with the results of *Lieberman* [1991], who considered the period from October to April. This study demonstrates that the P-A-2 mode plays a critical role in the stratosphere during the NH summer.

Finally, we discuss the relationship between tides and diabatic heating. Figure 5b shows the seasonal variations of the Hough modes in terms of the diabatic heating rate averaged between 500 hPa and 100 hPa. Symmetric modes attain maxima at equinox, while antisymmetric components become maximal during the NH summer. Convection and solar heating mainly contribute to the total heating rates (not shown). Zonally uniform heating may be partially explained by Sun-synchronous heating, with its amplitude modulated by the land-sea distribution with a wave number of 1 (e.g., S15). Another possible candidate for the generation of the convective heating rate is the difference in precipitation patterns between land and ocean. Precipitation maxima occur in the afternoon/evening over continents and early in the morning over the oceans [e.g., *Dai et al.,* 2007], possibly generating a zonally uniform pattern on a UT basis.

We investigate how a very simple model based on classical tidal theory [*Chapman and Lindzen*, 1970] can capture the observed features, when it is driven by the prescribed heating rate from the JRA55. The vertical structure equation is solved for each Hough mode in the region between 0 km and 200 km altitude in log-pressure coordinate, with a vertical interval of 100 m. A static, frictionless atmosphere is assumed. The background-temperature profile is the average in the region between 30°S and 30°N up to 1 hPa, derived from the JRA-55 data. Above 1 hPa, the temperature is assumed to remain constant and identical to that at 1 hPa. The JRA55 heating rates in the troposphere (up to 20 km) are used as driving forces, with a zero stratospheric heating rate. Note that JRA55 heating rate is a function of altitude for each Hough mode.

Figure 5c shows the simulated seasonal variations in Hough mode amplitude. It is shown that even this simple classical model reproduces the dominance of P-A-2 mode during the NH summer. Thus, the dominance of the P-A-2 mode can be understood in terms of the excitation efficiency [e.g., *Horinouchi and Yoden*, 1996]. The theoretical vertical wavelengths of the P-S-1, P-S-2, P-A-1, and P-A-2 modes are 26 (52) km, 11 (22) km, 103 (206) km, and 15 (30) km, respectively, for $N^2 = 4.0 \times 10^{-4}$ (1.0×10^{-4}) in the stratosphere (troposphere). Thus, tropospheric heating with a depth of ~15 km efficiently excites the P-A-2 mode.

At the same time, we see a significant discrepancy between the observations and the model. While the observed P-A-2 amplitude during DJF is much smaller than that during JJA (Figure 5a), the simulated

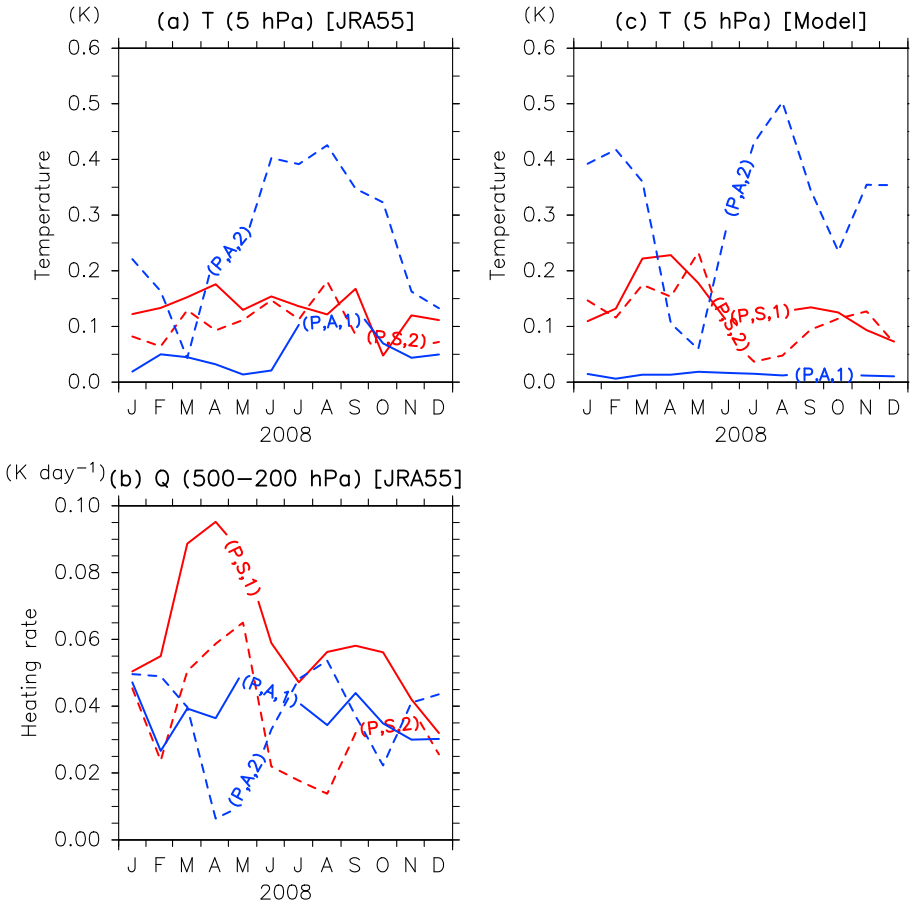

Figure 5. Seasonal variation in 2008 for the propagating Hough mode amplitude (i.e., $|C_n|$ in equation (1)) of the zonally uniform, diurnal tide for (a) temperature at 5 hPa and (b) diabatic heating rate averaged between 500 hPa and 200 hPa, derived from JRA-55 data. (c) As for Figure 5a but for the classical tidal model (see text for details). "S" and "A" denote symmetric and antisymmetric modes, respectively.

amplitude during DJF is comparable to that during JJA (Figure 5c). The seasonality of the diurnal migrating tides in the tropical stratosphere is affected by the latitudinal shear of the background zonal wind, which attains a maximum at solstice [*Sakazaki et al.,* 2013b]. In the MLT, nonlinear interactions are thought to be important as an excitation mechanism of zonally uniform tides [e.g., *Kuroda and Chiba*, 1995; *Hagan and Roble*, 2001]. A more realistic simulation including such "nonclassical" effects would be necessary in the future.

4. Summary

We have found significant zonally uniform tidal signals in the tropical stratosphere during the NH summer. The zonally uniform tides have a diurnal frequency and strong antisymmetric components with respect to the equator, with a vertical wavelength of ~15 km. These characteristics can be approximately explained by the dominant presence of a single Hough mode; i.e., the second, antisymmetric, propagating mode. The dominance of this mode during the NH summer can be roughly explained by the excitation efficiency, but a more realistic simulation is required to understand the significant seasonality.

Zonal mean quantities, such as the BDC, are often examined in climatological studies. The present study suggests that zonally uniform tides should be considered carefully in such studies. In particular, the amplitude of the vertical wind variation (1 mm s^{-1} at 70 hPa) is larger than the climatological ascent motion in the stratosphere (0.5 mm s^{-1} at 70 hPa), which means that the vertical wind changes its sign within a day. As noted by *Seviour et al.* [2012], the daily mean should be used for the accurate estimation of climatological zonal mean fields. One should also be careful when developing a zonal mean climatology from temporally sparse observational data.

Acknowledgments
We thank the SABER science team (Jim Russell) for providing the data used in this study (obtained by FTP from ftp://saber.gatsinc.com/custom/Temp_O3/). COSMIC data were obtained from the COSMIC Data Analysis and Archive Center (CDAAC). The JRA55 data are provided through the DIAS server from the JRA-55 project carried out by the Japan Meteorological Agency (JMA). The DIAS data set is archived and provided under the framework of the Data Integration and Analysis System (DIAS), through the National Key Technology, Marine Earth Observation Exploration System. We thank Masaaki Takahashi and Yuji Kuroda for useful suggestions related to this work. We are also grateful to two anonymous reviewers for their helpful comments for improving the manuscript. T. Sakazaki was supported in part by the Ministry of Education, Culture, Sports, Science and Technology (MEXT), Japan, through a grant-in-aid for JSPS Fellows (grant 25483400). M. Shiotani was also supported by MEXT through Grants-in-Aid for Scientific Research (25281006). All figures were drawn with the GFD-Dennou Library.

References

Anthes, R. A., et al. (2008), The COSMIC/FORMOSAT-3 Mission: Early results, *Bull. Am. Meteorol. Soc.*, *89*, 313–333, doi:10.1175/BAMS-89-3-313.

Chapman, S., and R. S. Lindzen (1970), *Atmospheric Tides*, 200 pp., D. Reidel, New York.

Chiba, M., and K. Shibata (1992), Zonally symmetric diurnal tides simulated with a general circulation model, *J. Meteorol. Soc. Jpn.*, *70*, 789–794.

Dai, A., X. Lin, and K.-L. Hsu (2007), The frequency, intensity, and diurnal cycle of precipitation in surface and satellite observations over low-and mid-latitudes, *Clim. Dyn.*, *29*, 727–744.

Eyring, V., et al. (2013), Overview of IGAC/SPARC Chemistry-Climate Model Initiative (CCMI) community simulations in support of upcoming ozone and climate assessments, *SPARC Newsl.*, *40*, 48–66.

Forbes, J. M., and D. Wu (2006), Solar tides as revealed by measurements of mesosphere temperature by the MLS experiment on UARS, *J. Atmos. Sci.*, *63*, 1776–1797.

Fueglistaler, S., A. E. Dessler, T. J. Dunkerton, I. Folkins, Q. Fu, and P. W. Mote (2009), Tropical tropopause layer, *Rev. Geophys.*, *47*, RG1004, doi:10.1029/2008RG000267.

Hagan, M. E., and R. G. Roble (2001), Modeling diurnal tidal variability with the National Center for Atmospheric Research thermosphere-ionosphere-mesosphere-electrodynamics general circulation model, *J. Geophys. Res.*, *106*(A11), 24,869–24,882, doi:10.1029/2001JA000057.

Horinouchi, T., and S. Yoden (1996), Excitation of transient waves by localized episodic heating in the tropics and their propagation into the middle atmosphere, *J. Meteorol. Soc. Jpn.*, *74*, 189–210.

Kobayashi, S., et al. (2015), The JRA-55 reanalysis: General specifications and basic characteristics, *J. Meteorol. Soc. Jpn.*, *93*, 5–48.

Kuroda, Y., and M. Chiba (1995), Creation of a zonally symmetric tide due to the interference of the migrating diurnal tide and a quasi-stationary wave, *J. Meteorol. Soc. Jpn.*, *73*, 737–746.

Lieberman, R. S. (1991), Nonmigrating diurnal tides in the equatorial middle atmosphere, *J. Atmos. Sci.*, *48*, 1112–1123.

Lieberman, R. S., and C. B. Leovy (1995), A numerical model of nonmigrating diurnal tides between the surface and 65 km, *J. Atmos. Sci.*, *52*, 389–409.

Marsh, D. R., M. J. Mills, D. E. Kinnison, J.-F. Lamarque, N. Calvo, and L. M. Polvani (2013), Climate change from 1850 to 2005 simulated in CESM1(WACCM), *J. Clim.*, *26*, 7372–7391, doi:10.1175/JCLI-D-12-00558.1.

Neale, R. B., J. Richter, S. Park, P. H. Lauritzen, S. J. Vavrus, P. J. Rasch, and M. Zhang (2013), The mean climate of the Community Atmosphere Model (CAM4) in forced SST and fully coupled experiments, *J. Clim.*, *26*, 5150–5168, doi:10.1175/JCLI-D-12-00236.1.

Oberheide, J., M. E. Hagan, R. G. Roble, and D. Offermann (2002), Sources of nonmigrating tides in the tropical middle atmosphere, *J. Geophys. Res.*, *107*(D21), 4567, doi:10.1029/2002JD002220.

Onogi, K., et al. (2007), The JRA-25 reanalysis, *J. Meteorol. Soc. Jpn.*, *85*, 369–432.

Russell, J. M., III, M. G. Mlynczak, L. L. Gordley, J. Tansock, and R. Esplin (1999), An overview of the SABER experiment and preliminary calibration results, *Proc. SPIE Int. Soc. Opt. Eng.*, *3756*, 277–288.

Sakazaki, T., M. Fujiwara, X. Zhang, M. E. Hagan, and J. M. Forbes (2012), Diurnal tides from the troposphere to the lower mesosphere as deduced with TIMED/SABER satellite data and six global reanalysis data sets, *J. Geophys. Res.*, *117*, D13108, doi:10.1029/2011JD017117.

Sakazaki, T., et al. (2013a), Diurnal ozone variations in the stratosphere revealed in observations from the Superconducting Submillimeter-Wave Limb-Emission Sounder (SMILES) on board the International Space Station (ISS), *J. Geophys. Res. Atmos.*, *118*, 2991–3006, doi:10.1002/jgrd.50220.

Sakazaki, T., M. Fujiwara, and X. Zhang (2013b), Interpretation of the vertical structure and seasonal variation of the diurnal migrating tide from the troposphere to the lower mesosphere, *J. Atmos. Sol. Terr. Phys.*, *105–106*, 66–80.

Sakazaki, T., K. Sato, Y. Kawatani, and S. Watanabe (2015), Three-dimensional structures of tropical nonmigrating tides in a high vertical resolution general circulation model, *J. Geophys. Res. Atmos.*, *120*, 1759–1775, doi:10.1002/2014JD022464.

Seviour, W. J. M., N. Butchart, and S. C. Hardiman (2012), The Brewer-Dobson circulation inferred from ERA-Interim, *Q. J. R. Meteorol. Soc.*, *138*, 879–888, doi:10.1002/qj.966.

Zou, C.-Z., H. Qian, W. Wang, L. Wang, and C. Long (2014), Recalibration and merging of SSU observations for stratospheric temperature trend studies, *J. Geophys. Res. Atmos.*, *119*, 13,180–13,205, doi:10.1002/2014JD021603.